TITLE

Adenylate Kinase 2 deficiency causes NAD+ depletion and impaired purine metabolism during myelopoiesis

AUTHORS

Wenqing Wang[1], Andew DeVilbiss[2], Martin Arreola[1], Thomas Mathews[2], Misty Martin-Sandoval[2], Zhiyu Zhao[2], Avni Awani[1], Daniel Dever[1], Waleed Al-Herz[3], Luigi Noratangelo[4], Matthew H. Porteus[1], Sean J. Morrison[2], Katja G. Weinacht[1, *]

1. Department of Pediatrics, Stanford University School of Medicine, Stanford, California 94305 USA

2. Children's Research Institute, University of Texas Southwestern Medical Center, Dallas, Texas 75390 USA

3. Department of Pediatrics, Faculty of Medicine, Kuwait University, Safat, 13110 Kuwait

4. Laboratory of Clinical Immunology and Microbiology, National Institute of Health, BETHESDA MD 20814 USA

* Corresponding author

ABSTRACT

Reticular Dysgenesis is a particularly grave from of severe combined immunodeficiency (SCID) that presents with severe congenital neutropenia and a maturation arrest of most cells of the lymphoid lineage. The disease is caused by biallelic loss of function mutations in the mitochondrial enzyme Adenylate Kinase 2 (AK2). AK2 mediates the phosphorylation of adenosine monophosphate (AMP) to adenosine diphosphate (ADP) as substrate for adenosine triphosphate (ATP) synthesis in the mitochondria. Accordingly, it has long been hypothesized that a decline in OXPHOS metabolism is the driver of the disease. The mechanistic basis for Reticular Dysgenesis, however, remained incompletely understood, largely due to lack of appropriate model systems to phenocopy the human disease. We have used single cell RNA-sequencing of bone marrow cells from 2 reticular dysgenesis patients to gain insight into the disease pathology. Gene set enrichment for differentially expressed genes in different subsets of myeloid and lymphoid progenitor cells pointed to processes involving RNA and ribonucleoprotein assembly and catabolism as well as cell cycle defects. To investigate these findings and precisely mimic the failure of human myelopoiesis in culture, we developed a cell-tracible model of Reticular Dysgenesis based on CRISPR-mediated disruption of the AK2 gene in primary human hematopoietic stem cells. In this model, we have identified that AK2-deficienct myeloid progenitor cells exhibit NAD+ depletion and high levels of reductive stress accompanied by an accumulation of AMP and IMP while ADP and ATP are only mildly decreased. Our studies further show that AK2-deficienct cells have decreased de novo purine synthesis and increased purine breakdown, accompanied by decreased RNA and ribosome subunit cellular content. These data highlight the profound impact of mitochondrial dysfunction on the cellular redox state and nucleotide pool and identify the mechanistic basis of Reticular Dysgenesis as a defect in purine metabolism.

INTRODUCTION

Reticular Dysgenesis defies the classical patterns of hematopoietic failure and immunodeficiency syndromes in many ways. The disease is defined by a combined and complete maturation arrest of the myeloid and lymphoid lineages[1,2] while the bone marrow cellularity is preserved, sometimes increased[3]. In addition, patients suffer from sensorineural hearing loss[1,2]. The disease is invariably fatal early in life unless hematopoietic and immune reconstitution are achieved by hematopoietic stem cell transplantation[4]. The predominance of opportunistic bacterial and fungal infections suggests that the neutropenia is the prevailing cause of early death4. Reticular Dysgenesis is caused by defects in the mitochondrial enzyme Adenylate Kinase 2[1,2].

Interestingly, none of the classic mitochondriopathies caused by respiratory chain defects present with numeric or functional defects in the myeloid or lymphoid lineages[5].

Adenylate Kinases are a group of at least 9 phosphotransferases that maintain adenine nucleotide homeostasis, i.e. the ratio between AMP, ADP and ATP in defined compartments of the cell[6–8]. Shuttle networks allow for the redistribution of AMP and ADP between spatially distinct locations of energy production and energy demand across the nucleotide-permeable outer mitochondrial membrane[6,7,9,10]. AK2 is localized in the mitochondrial intermembrane space where is catalyzes the reversible reaction AMP+ATP<->2ADP. ADP is then actively transported to the mitochondrial matrix by the ADP/ATP translocase where it is phosphorylated to ATP by the ATP synthase. AK2 is ubiquitously expressed while the expression of its cytosolic counterpart AK1 follows a tissue/cell type restricted pattern2. AK1 promotes the same enzymatic reaction as AK2, albeit at a lower rate (AK2 Km(AMP) <10uM vs AK1 Km(AMP) 100-200mM)[6]. Because ADP is continuously removed from the intermembrane space while AMP and ATP are actively repleted, AK2 promotes the conversion of AMP and ATP to ADP. In the cytosol, the relative substrate concentrations are the reverse. Because ATP is continuously consumed while AMP is generated, AK1 mediates the conversion of ATP and AMP to ADP.

Although AK2 is ubiquitously expressed, non-hematopoietic tissues other than the stria vascularis in the inner ear are largely unaffected by AK2 deficiency[1,2]. This indicates that most cells do not depend on AK2 function. Within the hematopoietic system, platelets, erythrocytes, and some B cells develop to maturity. Why AK2 is indispensable in some hematopoietic and immune cells but not in other is unclear. Interestingly, AK1 is not expressed in many hematopoietic and immune cells2. It has been speculated that the tissue specific phenotype of Reticular Dysgenesis stems from a lack of redundancy of AK1 and AK2 in affected cell types and that AK1 may at least in part compensate for the lack of AK2 in cells in which both kinases are expressed[2,11,12].

While the genetic underpinnings of Reticular Dysgenesis have been known for over a decade, the molecular and cellular basis for the combined failure of myelopoiesis and lymphopoiesis is less clear. Cells have a myriad of redundantly ADP-producing pathways and the specific cells types that are predominantly affected by Reticular Dysgenesis, neutrophils and T cells, are known to rely heavily on glycolysis as baseline and under stress[13–18]. Therefore, alternate drivers of disease pathology should be investigated in disease models that faithfully recapitulate the human disease.

MATERIAL AND METHODS

Subjects

Consent was obtained according to Boston Children’s Hospital IRB.

Single cell RNA-seq

Bone marrow samples from two Reticular Dysgenesis patients were obtained and treated with ammonium chloride solution (StemCell Technologies 07850) for the lysis of red blood cells. Single cell RNA-seq libraries were constructed from FACS sorted CD45+ bone marrow cells, using Chromium Single Cell 3' GEM, Library & Gel Bead Kit v3 (10X Genomics). Libraries were sequenced on Illumina NextSeq 500. In addition, bone marrow scRNA-seq data from eight human healthy donors were downloaded from Human Cell Atlas[19]. Reads alignment to human genome hg19, cell barcode calling and UMI count were performed using cellranger 3.0.0 (10X Genomics). Clustering analysis and differential gene expression were performed using Seurat v3[20].

Cell culture

Human cord blood CD34+ HSPCs were either purchased from StemCell Technologies (78003) or acquired via the Binns Program for Cord Blood Research at Stanford University from donors under informed consent. Human fetal liver CD34+ HSPCs were isolated from fetal liver tissues acquired via Advanced Bioscience Resources

from donors under informed consent. For CD34+ HSPC in vitro expansion, cells were cultured in StemSpan SFEMII (StemCell Technologies 09655) supplemented with 100µg/mL SCF (StemCell Technologies 78062), 100µg/mL TPO (StemCell Technologies 78210.1), 100µg/mL FLT3L (StemCell Technologies 78009), 100µg/mL IL-6 (StemCell Technologies 78050), 35nM UM171 (StemCell Technologies 09655) and 0.75µM StemReginin 1 (StemCell Technologies 72342), at 37°C, 5% O2 and 5% CO2.

For in vitro granulocyte differentiation, CD34+ HSPCs were cultured in Myelocult H5100 (StemCell Technologies 05150) supplemented with 100µg/mL SCF, 100µg/mL IL-3 (StemCell Technologies 78040), 10µg/mL G-CSF (NEUPOGEN, Amgen) and 1µM hydrocortisone (Sigma H0888) at 37°C and 5% CO2. To analyze the effect of purine imbalance on HSPC differentiation, CD34+ HSPCs were differentiated in MEM alpha either with or without nucleosides (Thermo Fisher 32571-036 and 32561-037) supplemented with 10% dialyzed FBS (Thermo Fisher, A3382001), SCF, IL-3, G-CSF and hydrocortisone. MEM alpha is the base media of Myelocult H5100. Adenosine (Sigma A4036) or guanosine (Sigma G6264) was supplemented in Myelocult media at 40mg/L. AMPD inhibitor (Sigma 5.33642) was supplemented at 20µM.

rAAV6 production

AAV vector plasmids were cloned in the pAAV-MCS plasmid containing ITRs from AAV serotype 2 (AAV2). Vectors contain an SFFV promoter, GFP or BFP reporter gene, BGH polyA, and left and right homology arms (400bp each) specific to AK2 or AAVS1 CRISPR editing sites. pDGM6 plasmid, containing the AAV6 cap genes, AAV2 rep genes, and adenovirus helper genes, was a gift from David Russell. rAAV6 particles were either produced by Vigene or as described with modifications[21]. Briefly, 293T cells grown to 70-80% confluency in each 15cm dish were transfected with 6µg ITR-containing plasmid and 22µg pDGM6 using 112µg acidified PEI (Polysciences, 23966-1). 48-72 hours after transfection, cells were harvested and rAAV6 particles were purified using an AAVpro Purification Maxi kit (Takara, 6666) according to manufacturer's protocol. rAAV6 titer was quantified by qRT-PCR[22].

CRISPR/Cas9 gene editing

CD34+ HSPCs were CRISPR edited at AK2 or AAVS1 locus 3 days after thawing or isolation. Synthetic sgRNAs were purchased from Synthego. sgRNA sequences targeting AK2 or AAVS1 locus are: AK2, UUCCUGUUCUCAGAUCACCG; AAVS1, GGGGCCACUAGGGACAGGAU. For 1 million CD34+ HSPCs, 8µg sgRNA and 15µg Cas9 (IDT, 1081059) were mixed and incubated at room temperature for ~15 minutes to form RNP complex. RNP was delivered by electroporation using a Lonza 4D-nucleofector and P3 Primary Cell Kit (Lonza, V4XP-3012). Immediately after electroporation, cells were transferred to fresh StemSpan media and corresponding AAV with GFP and BFP reporters were added to cell culture at the MOI of 50,000 each. Cells were cultured for 2-3 days before FACS enrichment for lin-CD34+GFP+BFP+ cells.

Flow cytometry and cell sorting

The following antibodies were used for flow cytometry analysis and cell sorting of human bone marrow samples: CD117 PE (Biolgend 323408), CD16 PE-CF594 (BD 562293), CD33 PE-Cy7 (BD 333946), siglet-8 APC (Biolegend 347105), HLA-DR APC-R700 (BD 565127), CD14 APC-Cy7 (Biolgend 367108), CD11b BV605 (Biolgend 301332), CD3 BV650 (Biolgend 317324), CD19 BV650 (Biolgend 302238), CD56 BV650 (Biolgend 362532), CD34 BV711 (BD 740803), CD45 BV785 (Biolgend 304048), and CD15 BUV395 (BD 563872). The following antibodies were used for cell sorting of lin-CD34+GFP+BFP+ HSPCs after CRISPR editing: CD34 APC (Biolegend 343510), CD11b APC-Cy7 (Biolegend 301342), CD14 APC-Cy7 (Biolegend 367108), CD15 PE (Biolegend 323006), and CD16 PE (Biolegend 360704). The following antibodies were used for flow cytometry analysis of myeloid differentiation and cell sorting of PMs, MCs and NPs: CD16 APC (Biolegend 302012), HLA-DR APC-Cy7 (Biolegend 307618), CD11b PE (Biolegend 301306) or BV711 (Biolgend 301344), CD117 PE-Cy7

(Biolegend 323408), and CD15 BV785 (Biolegend 323044). Cell sorting were performed on BD FACSAria II or FACSAria Fusion. Data analysis was done on Flowjo v10.

Western blot

Primary antibodies used for Western blot of β-actin and AK2 proteins were: anti-actin (Santa Cruz Biotechnology sc-47778, 1:1000 dilution), anti-AK2 (ProteinTech 11014-1-AP, 1:200 dilution). Secondary antibodies were: m-IgGκ BP-HRP (Santa Cruz Biotechnology sc-516102, 1:5000 dilution), mouse anti-rabbit IgG-HRP (Santa Cruz Biotechnology sc-2357, 1:5000 dilution).

Metabolomics

Cell sorting for metabolomics analysis was carried out as described[23]. Briefly, cells were sorted on a FACSAria Fusion sorter running with a sheath fluid of 0.5X PBS, and a 70-µm nozzle to minimize the volume of sorted drops. For each sample, 10,000 cells were sorted directly into 40µL acetonitrile. Samples were vortexed for 1 min to lyse the cells, then centrifuged at 17,000g for 15 min at 4 °C, and supernatant was transferred to a fresh tube and stored at -80°C. Metabolites were quantified on a Quadrupole-Orbitrap mass spectrometer (Thermo Fisher).

RNA-seq

RNA was extracted from sorted PMs, MCs and NPs using a Qiagen RNeasy Plus Micro kit. RNA-seq library was constructed with a Takara SMARTseq v4 kit, and sequenced on Illumina NovaSeq. Reads mapping to human genome hg38, transcript quantification and TPM calculation were performed using Kallisto v0.46.0[24]. Differential gene expression was analyzed by DESeq2[25].

Seahorse mitochondrial stress test

Real-time cell metabolic analysis was performed on a Seahorse XFe96 Analyzer (Agilent) using a Seahorse XF Cell Mito Stress Test kit (Agilent 103015-100) according to manufacturer's protocol. A 96-well Seahorse cell-culture plate was coated with 0.1mg/mL Poly-D-Lysine (Advanced Biomatrix 5174). Sorted PMs, MCs and NPs were pelleted and resuspended in Seahorse XF RPMI media (Agilent 103576-100). 80,000-100,000 cells were plated in each well. Each cell type/treatment were plated in at least triplicate. Oligomycin (final concentration 1.5uM), FCCP (final centration 1uM) and rotenin/antimycin A (final concentration 0.5uM each) were injected into cell culture media sequentially during the assay.

Mitochondrial copy number assay

Genomic DNA was extracted using a Qiagen DNeasy Blood and Tissue kit. qPCR quantification of mitochondrial copy number was performed as described[26]. Primers and probes (purchased from IDT) used for the nuclear B2M and mitochondrial MT-ND1 genes are: B2M-F, CCAGCAGAGAATGGAAAGTCAA; B2M-R, TCTCTCTCCATTCTTCAGTAAGTCAACT; B2M-P, /56-FAM/ ATGTGTCTG /ZEN/ GGTTTCATCCATCCGACA /EIABkFQ/; MT-ND1-F, CCCTAAAACCCGCCACATCT; MT-ND1-R, GAGCGATGGTGAGAGCTAAGGT; MT-ND1-P, /56-FAM/ CCATCACCC /ZEN/ TCTACATCACCGCCC /3IABkFQ/

Mitochondrial membrane potential

To quantify mitochondrial membrane potential, cells were resuspended in PBS with 20nM TMRM (Thermo Fisher T668) following surface marker antibody staining, incubated at 37°C and 5% CO2 for 1 hour, and then analyzed by flow cytometry.

rRNA content

rRNA content was quantified by Pyronin Y staining. Cells were counted and 500,000 cells were plated in 1mL fresh Myelocult media. Hoechst 33324 (ThermoFisher H3570) was added to the media at the concentration of 5µg/mL, and cells were incubated at 37°C and 5% CO2 for 30 minutes. Pyronin Y (Sigma P9172) was then added at the concentration of 0.5µg/mL, and cells were incubated for an additional 45 minutes. Afterwards, cells were stained with surface marker antibodies and analyzed by flow cytometry.

Nascent peptide synthesis

Click-iT™ Plus OPP Alexa Fluor™ 594 Protein Synthesis Assay Kit (Thermo Fisher C10457) was used to quantify nascent peptide synthesis. Cells were counted and 500,000 cells were plated in 1mL fresh Myelocult media supplemented with 20µM OP-puromycin. After 1 hour incubation at 37°C and 5% CO2, cells were stained with surface marker antibodies, and proceeded with click reaction for OP-puromycin staining according to manufacturer's protocol. Cells were then analyzed by flow cytometry.

Statistical Analysis

p values were determined by two way ANOVA with Tukey's post-test, paired or unpaired Student's t test using R/Bioconductor. Differences were considered statistically significant when $p < 0.05$ (* $p < 0.05$, ** $p < 0.01$, *** $p < 0.001$, ****$p < 0.0001$, ns not significant).

Data Availability

Single cell RNA-seq data was deposited in GEO with accession number GSE179346. RNA-seq was deposited in GEO with accession number GSE179320.

RESULTS

Single cell RNA sequencing of Reticular Dysgenesis patient bone marrow

To glean insights into the mechanistic basis of Reticular Dysgenesis, we performed single cell RNA sequencing (scRNA-seq) on bone marrow samples of 2 previously reported patients with biallelic c. 542G>A , 524G>A mutation[4,11,12]. Myeloid differentiation defects of RD patients was confirmed by flow cytometry (Fig 2A, B). In the myeloid compartment (CD3- CD19- CD56-), RD patients showed significantly lower commitment to the HLA-DR- granulocytic lineage, and severe maturation arrest at the CD117+ promyelocyte stage. We used published bone marrow scRNA-seq data from 8 healthy donors as a control group[19]. Unsupervised clustering identified 22 cell populations (Fig 1A, Fig S1). Mature neutrophils were not captured in our scRNA-seq data or the published data, due to limitations of droplet-based 10X scRNA-seq platform, as neutrophil's high levels of RNase and proteinase would digest the RNA and enzymes in the droplets. As expected, RD patient bone marrow comprises significantly larger percentages of cells in the HSPCs clusters (HSC, CMP, CLP and ProB), whereas more mature populations across myeloid and lymphoid lineages, decreased. Monocytes, T cells and NK cells showed the most significantly reduced frequency (Fig 1B, C). RD patient samples showed relatively normal erythroid development (Fig 1B, C), possibly due to the compensatory AK1 activities, which is expressed in the erythroid lineage, but not in the HSPC, myeloid or lymphoid populations (Fig 1D). We performed

differential gene expression analysis in HSPC clusters comparing RD patients to healthy donors, which revealed highly overlapping enriched pathways in the down-regulated genes (Fig 1E). The top 10 down-regulated pathways in HSPC clusters include multiple pathways involved in RNA metabolism, RNP complex biogenesis and cell cycle progression are down-regulated in RD patients (Fig 1E), suggesting that defective nucleotide metabolism may significantly contribute to the mechanism of RD immunodeficiency and neutropenia.

A Cell-traceable Model of Reticular Dysgenesis in Human Hematopoietic Stem Cells

A numbers of strategies have been explored to model RD. Prior studies using a zebrafish Ak2-knockout model and AK2-deficient iPSCs[12] do not fully recapitulate definitive human hematopoiesis; whereas germline[27] or lineage-specific depletion of Ak2 with Vav-Cre (Karl Welte, personal communication) in mice are embryonic lethal before the onset of myelopoiesis. To overcome these limitations, we development a biallelic AK2 knock-out model in primary human hematopoietic stem and progenitor cells (HSPCs). We combined CRISPR/Cas9 gene editing with adeno-associated viral vector delivery of two homologous donors containing GFP and BFP reporters[21,28] (Fig 3A), to disrupt the AK2 gene at the catalytic domain, LID domain, and to allow selection of biallelic edited cells (GFP+ BFP+) by FACS sorting (Fig 3B). AK2 knock-out in the GFP+BFP+ fraction of edited HSPCs was confirmed by Western blot (Fig 3C). Cells edited at the safe harbor locus AAVS1[29] were used as a control. AK2$^{-/-}$ and AAVS1$^{-/-}$ HSPCs were differentiated in an in vitro culture along the granulocytic lineage. Consistent with RD patient presentation (Fig 2), AK2$^{-/-}$ HSPCs showed decreased commitment to the HLA-DR- granulocyte lineage (Fig 3D,E), differentiation arrest at the promyelocyte stage (PMs, CD15- CD117+), and failure to further mature into myelocytes (MCs, CD15+ CD11b+ CD16-) and neutrophils (NPs, CD15+ CD11b+ CD16+) (Fig 3D, F). Additionally, proliferation of AK2$^{-/-}$ HSPCs was severely compromised (Fig 3G), resulting in significantly lower yield of MCs and NPs (Fig 3H). These results demonstrated that the AK2 biallelic knock-out HSPC model is capable of recapitulates the RD myelopoiesis failure in vitro.

Energy metabolism and protein synthesis peak at the PM stage

To understand why AK2 depleted HSPCs fail to develop past the PM stage, we first sought to investigate how energy metabolism patterns change during normal myelopoiesis. Using a Seahorse cell metabolic analyzer, we quantified mitochondrial respiration and glycolysis rate on control PMs, MCs and NPs (Fig 4A-B). Baseline mitochondrial respiration, maximal respiration and spare respiratory capacity all steadily decease from the PM stage to mature NPs (Fig 4C-E). These data are consistent with the observation that mitochondrial copy number also deceases during NP maturation (Fig 4G). In addition, glycolysis rate is also significantly lower in NPs compared with PMs and MCs (Fig 4B, F).

As ribosomal biogenesis is often the most energy consuming process of a cell[30], and ribosomopathy commonly affect the function of HSC and erythroid progenitors[31,32], we asked how ribosomal activities are regulated during neutrophil maturation. RNA-seq revealed that ribosomal subunit gene expression decreases from PMs to NPs (Fig 4H). While Pyronin Y staining showed that MCs contain the highest amount of ribosomal RNA content (Fig 4I), nascent peptide synthesis rate as quantified by OP-puromycin staining suggest that PMs are the most active in protein synthesis (Fig 4J). Together, these data showed that PMs are the most energetically active stage during myelopoiesis, which leads us to hypothesize that energy metabolism defects in AK2 depleted PMs may lead to the maturation arrest.

AK2 depletion causes AMP accumulation and NAD+ depletion

To understand the metabolic consequences of AK2 deficiency, we performed metabolomics profiling in AK2$^{-/-}$ and AAVS1 PMs, MCs and NPs. As expected, AK2 depletion increases AMP levels and AMP/ADP and AMP to ATP ratios at MC and NP stages (Fig 5A), suggesting that ATP production is compromised in AK2$^{-/-}$ cells.

Unexpectedly, we also observed a decrease in NAD+ levels, and a significant increase in NADH/NAD+ ratio (Fig 5B). The increase in NADH/NAD+ ratio suggests an excess of reducing equivalents in AK2$^{-/-}$ cells, which is corroborated by an increase in the ratio of reduced to oxidized glutathione (GSH/GSSG) (Fig 5C). The AMP accumulation and redox imbalance progressively worsen as cells mature. Ak2$^{-/-}$ MCs and NPs also showed an increase in the glycolytic metabolites glucose 6-phosphate and phosphoenolpyruvate (PEP), but a decrease in the TCA cycle metabolite malate (Fig 5D), suggesting that mitochondrial metabolism may be compromised.

Mitochondrial metabolism is compromised in AK2 depleted promyelocytes

To further explore the mitochondrial metabolic defects caused by AK2 depletion, we focused on the metabolically active PM stage and analyzed mitochondrial respiration and glycolysis in AK2$^{-/-}$ and AAVS1$^{-/-}$ cells, (Fig 6A, B). AK2$^{-/-}$ PMs exhibit a lower baseline respiration (Fig 6C), but normal maximal respiration and spare respiratory capacity upon FCCP uncoupling (Fig 6D, E). Glycolysis rate slightly increases in AK2$^{-/-}$ PMs (Fig 6F). Furthermore, AK2$^{-/-}$ PMs and MCs showed no change in mitochondrial copy number compared to AAVS1$^{-/-}$ cells (Fig 6G). Interestingly, mitochondrial membrane potential is higher in AK2$^{-/-}$ PMs compare to control (Fig 6H). Mitochondrial membrane potential is maintained by Complex I and Complex III activities and used as the energy source to drive ATP synthase. As the spare respiratory capacity indicates the ability of mitochondria to meet extra energy demands beyond the baseline level, these data suggest that the lower baseline respiration in AK2$^{-/-}$ PMs was not caused by defective electron transport chain (ETC) capacity. Rather, it raises the possibility that the increase in membrane potential is the result of a decrease in ATP production. Notably, Complex I accepts a pair of electrons from NADH, passing them to coenzyme Q, while converting NADH to NAD+. Decreased flux through ETC in AK2 depleted PMs may impede the regeneration of NAD+ at Complex I, causing the increase in NADH/NAD+ ratios at later differentiation stages.

AK2 depletion impairs purine metabolism and protein synthesis

Previous reports on ETC defective cells indicated aspartate deficiency and purine auxotrophy as the cause of the cell proliferation defect[33,34], as NAD+ serves as an important cofactor during aspartate and purine biosynthesis. In AK2 depleted cells, we observed a severe depletion of aspartate (Fig 7A), and significant accumulation of IMP (Fig 7B). Purine is the building block of DNA and RNA. Defects in purine metabolism are known causes of immunodeficiency with myeloid maturation defects[35,36]. Single cell RNA-seq data of RD patients pointed to defective ribosomal biogenesis in HSPC populations. As ribosomal RNA (rRNA) constitutes >85% of cellular RNA content[37], we asked whether RNA synthesis is compromised by AK2 depletion. Indeed, the majority of ribosomal subunit genes are trending towards down-regulation in AK2$^{-/-}$ PMs and MCs. (Fig 7C). Furthermore, rRNA contents in AK2$^{-/-}$ MCs and NPs are significantly lower than that of the respective controls (Fig 7D), and protein synthesis rate is decreased in AK2$^{-/-}$ PMs (Fig 7E).

Purine imbalance is detrimental to neutrophil differentiation

We next explored whether defective purine biosynthesis is responsible for AK2$^{-/-}$ myelopoiesis defects. Under normal physiological conditions, most of the cellular purine pool is derived from the recycling of degraded bases via the salvage pathway[38]. This process is fast and energy efficient. Under cellular conditions of increased purine demand, the *de novo* purine biosynthetic pathway is utilized[39–42]. The de novo pathway is an energy-intensive pathway that generates IMP from PRPP, amino acids, formate and CO2. In the final 2-step reaction, IMP is converted to GMP and AMP, under consumption of NAD+ and aspartate, respectively. In this study, the regularly used culture media was rich in purine precursors, as nucleosides are present in both the base media and the serum. To investigate whether de novo purine biosynthesis is compromised in AK2$^{-/-}$ cells, we differentiated AK2$^{-/-}$ and AAVS1$^{-/-}$ HSPCs in MEM alpha with or without nucleosides, and supplemented with 10% dialyzed FBS (see Material and Methods). Surprisingly, differentiating AK2$^{-/-}$ HSPCs in purine-depleted media did not further exacerbate the proliferation or neutrophil maturation defects, nor does it impact

the differentiation of control AAVS1$^{-/-}$ HSPCs (Fig 8A, B), suggesting that both AK2$^{-/-}$ and AAVS1$^{-/-}$ HSPCs are capable of de novo purine biosynthesis to support DNA and RNA synthesis. However, supplementing only adenosine or guanosine, in contrast to a balanced mix of nucleosides and deoxynucleosides (including adenosine, deoxyadenosine, guanosine, deoxyguanosine, cytidine, deoxycytidine, thymidine and uridine), was shown to be extremely detrimental to the proliferation of AAVS1$^{-/-}$ HSPCs (Fig 8C, D). Adenosine supplementation did not exacerbate AK2$^{-/-}$ proliferation defects, but guanosine supplementation also severely impairs AK2$^{-/-}$ HSPC proliferation (Fig 8C, D). These data suggested that purine imbalance, rather than purine deficiency, is detrimental to neutrophil differentiation.

These data also raised the question of the source of IMP accumulation in AK2$^{-/-}$ MCs and NPs, as AK2 depleted cells are capable of synthesizing purines from PRPP. Other sources of IMP production include ITP hydrolysis by ITPase, salvage of hypoxanthine by HPRT, and AMP deamination by AMPD. We then examined whether AK2$^{-/-}$ cells converts excess AMP to IMP as a mechanism to avert AMP toxicity. AAVS1$^{-/-}$ HSPCs treated with AMPD inhibitor[43,44] showed a small decrease in proliferation, and no effect on proliferation was observed in AK2$^{-/-}$ HSPCs (Fig 8E, F). LC/MS/MS of AAVS1$^{-/-}$ and AK2$^{-/-}$ cells treated with AMPD inhibitor showed a significant decrease of IMP levels, compared with respective DMSO treated control (Fig 8G). No change in AMP levels was observed in AK2$^{-/-}$ MCs or NPs, but AMP levels increased in AAVS1$^{-/-}$ NPs following AMPD inhibitor treatment (Fig 8H). These data indicated that AMP deamination is a major source of IMP accumulation in AK2 depleted MCs and NPs.

DISCUSSION

Our studies showed that AK2 deficiency during myelopoiesis causes reductive stress and perturbations in ribonucleotide synthesis, assembly and breakdown that manifest in arrested maturation and significantly reduced proliferation of AK2-deficient HSPCs. Because histologic examinations of patient bone marrow can only visualize the maturation arrest, the hypo-proliferative phenotype of Reticular Dysgenesis has largely evaded awareness and investigation.

Pharmacologic interference with purine metabolism is recognized as a highly effective antiproliferative strategy. In addition, defects in purine catalyzing enzymes have long been recognized as a cause of SCID, such as loss-of-function mutations in adenosine-deaminase (ADA) and purine nucleotide phosphorylase (PNP) which selectively impair the growth and function of T cells. In ADA and PNP deficient patients, deoxyadenosine and deoxyguanosine, respectively, are not metabolized but instead are excreted into the plasma by dividing non-lymphoid cells. The deoxynucleosides are selectively phosphorylated and trapped inside T-lymphocytes, were they progressively accumulate intracellularly, inhibiting the enzyme ribonucleotide reductase, and thereby DNA synthesis[39,41,42,45–47]. In contrast, the ribonucleotide levels and excretion in ADA-deficient patients are normal because adenosine can be phosphorylated to AMP, converted to IMP and further to inosine and then excreted[39,45,46,48].

Analogous to the accumulation of deoxyadenosine in ADA SCID that inhibits ribonucleotide reductase activity, the AMP burden in AK2-deficiency overwhelms the capacity of its downstream catabolic enzymes AMP-deaminase and 5’ cytosolic nucleotidase II (NT5C2) leading to AMP and IMP accumulation, respectively. AMP and IMP control the de novo purine synthesis pathway by feedback inhibition of PRPP amidotransferase (PPAT) activity[40,49], thereby causing defects in replication, cell cycle, RNA synthesis and ribosome biogenesis which manifest in the observed arrest of proliferation and maturation. AMP and IMP catabolizing enzymes play important roles in health and disease. Human AMP-deaminase has at least 3 different isoforms (AMPD1/2/3) with cell and tissue specific distribution pattern[50]. While AMPD1 is enhanced in heart and skeletal muscle[50–52], AMPD2 and 3 show redundancy in most hematopoietic and immune cells (Human Protein Atlas). Recently, loss of function mutations in the erythrocyte-enhanced AMPD3 has been reported to cause T cell lymphopenia in mice[53]. Interestingly, gain of function mutations 5’ cytosolic nucleotidase II (NT5C2) are among the most frequently found mutations in relapsed ALL. NT5C2 mutations are present in 20% of relapsed T-ALLs and 3-10% of relapsed B-ALLs and present as heterozygous gain of function alleles exhibiting increased nucleotidase activity (Chelsea Diek, Doctorate Dissertation, Columbia University, 2019). The gain of function

phenotype is further implicated in drug resistance to thiopurine based chemotherapy[54,55]. These observations highlight that tissue specific expression patterns of purine metabolizing enzymes play an important role in defining the characteristic, lineage specific patterns of disease phenotypes.

As such, further investigations into the relationship between AK1 and AK2 are in order. AK1 and AK2's catalytic activities are reversible and solely driven by surrounding substrate and product concentration[6,7]. Accordingly, an increase in cytosolic AMP levels would eventually result in AK1 phosphorylating AMP to ADP. Nucleotides can permeate the outer mitochondrial membrane, leading to a redistribution of nucleosides between cytoplasm and mitochondria. These considerations are in support of the hypothesis AK1 can restore (to some extend) the nucleotide imbalance that results from AK2 deficiency. This hypothesis is further supported by a recent report showing that AK2 knockdown by short hairpin-RNA in primary T-ALL samples that didn't express AK1 led to apoptosis while B-ALL samples with higher expression of AK1 were less susceptible to apoptosis induction by AK2 shRNA-knockdown[56]. However, another study of AK2 knockdown by short hairpin-RNA in HSPCs did not demonstrate rescue of hematopoiesis by overexpressing AK1[56,57]. This raises the possibility that AK2 is dispensable in cells that physiologically express AK1, while AK1 may or may not be able to compensate for loss of AK2 in cells in which AK1 is dispensible[56].

The dynamic role of OXPHOS during myeloid development adds another layer of complexity. OXPHOS utilization peaks at the PM stage. Accordingly, this is when most of the AMP burden begins to accumulate. As MCs begins terminal differentiation and exit cell cycle, metabolites that cannot permeate the cell membrane build up. This may explain why hematopoietic stem and early progenitor cells of all lineages that rely less on OXPHOS and continuously divide are not affected by AK2 deficiency regardless of their expression of AK1.

Mitochondrial function and purine synthesis are intimately intertwined. Recently, it was reported that the six enzymes responsible for de novo IMP biosynthesis (PPAT, GART, FGAMS, PAICS, ADSL and ATIC) cluster near mitochondria in complexes referred to as "purinosomes" that are induced under conditions of high purine demand. It is believed that enzymatic clustering helps condense substrates and make their transfer more efficient[38,58]. Treatment with ETC and OXPHOS inhibitors increases purinosome assembly[59]. AK2 operates at the intersection between energy, redox and nucleotide homeostasis. In the context of AK2-deficiency, the system becomes unhinged and leads to metabolic escape mechanisms, most notably, reductive stress.

Reductive stress is marked by an accumulation of reducing species, such as an increased NADH/NAD+ ratio and can arise from defects in the electron transport chain (ETC) that prevent the cell from regenerating NAD+ from NADH. Our seahorse studies do not suggest that AK2-deficient cells have primary defects in electron transport, indicated by their normal to mildly increased reserve respiratory capacity. Instead, our studies indicate that AK2 deficient cells have an increase in membrane potential. It is possible that decrease in ATP production leads to an increase in membrane potential as less proton motive force is consumed to drive ATP-synthase activity. Recently, the role of NAD+ depletion during decreased ATP utilization and "overstretching of the mitochondrial membrane potential has been reported[60,61]. It has been suggested that the increase in membrane potential curtails the proton flux through ETC complex I and thereby decreases the regeneration of NAD+ from NADH and net electron transport.

For the past 60 years, the scientific community has examined disturbances in redox balance through the lens of oxidative stress[62,63]. Only in the last few years have concepts and mechanisms related to reductive stress emerged[64,65]. Our metabolomics studies indicate that AK2-deficient myeloid progenitors display a decrease in mitochondrial metabolites, including TCA cycle intermediaries and aspartate, while lipid carnitines were increased. These observations raise the possibility that mitochondrial reductive stress, curtails TCA cycle activity and diverts carbon and electron pools into lipid synthesis. A novel subpopulation of mitochondria attached to lipid droplets, deemed peri-droplet mitochondria, has recently been described[66]. Their biology is unknown. The study of AK2 deficiency allows us to dissect the link between mitochondrial function, reductive stress, purinosome activity and lipid metabolism. Further work will be necessary to define the mechanistic basis of metabolic escape due to AK2 deficiency and/or reductive stress and strategies to mitigate it.

REFERENCE

1. Lagresle-Peyrou, C. *et al.* Human adenylate kinase 2 deficiency causes a profound hematopoietic defect associated with sensorineural deafness. *Nat. Genet.* **41**, 106–111 (2009).

2. Pannicke, U. *et al.* Reticular dysgenesis (aleukocytosis) is caused by mutations in the gene encoding mitochondrial adenylate kinase 2. *Nat. Genet.* **41**, 101–105 (2009).

3. Hoenig, M., Pannicke, U., Gaspar, H. B. & Schwarz, K. Recent advances in understanding the pathogenesis and management of reticular dysgenesis. *Br. J. Haematol.* **180**, 644–653 (2018).

4. Hoenig, M. *et al.* Reticular dysgenesis: international survey on clinical presentation, transplantation, and outcome. *Blood* **129**, 2928–2938 (2017).

5. Vafai, S. B. & Mootha, V. K. Mitochondrial disorders as windows into an ancient organelle. *Nature* **491**, 374–383 (2012).

6. Dzeja, P. & Terzic, A. Adenylate kinase and AMP signaling networks: metabolic monitoring, signal communication and body energy sensing. *Int. J. Mol. Sci.* **10**, 1729–1772 (2009).

7. Dzeja, P. P. & Terzic, A. Phosphotransfer networks and cellular energetics. *J. Exp. Biol.* **206**, 2039–2047 (2003).

8. Amiri, M., Conserva, F., Panayiotou, C., Karlsson, A. & Solaroli, N. The human adenylate kinase 9 is a nucleoside mono- and diphosphate kinase. *Int. J. Biochem. Cell Biol.* **45**, 925–931 (2013).

9. Dzeja, P. P., Bast, P., Pucar, D., Wieringa, B. & Terzic, A. Defective metabolic signaling in adenylate kinase AK1 gene knock-out hearts compromises post-ischemic coronary reflow. *J. Biol. Chem.* **282**, 31366–31372 (2007).

10. Janssen, E., Terzic, A., Wieringa, B. & Dzeja, P. P. Impaired intracellular energetic communication in muscles from creatine kinase and adenylate kinase (M-CK/AK1) double knock-out mice. *J. Biol. Chem.* **278**, 30441–30449 (2003).

11. Henderson, L. A. *et al.* First reported case of Omenn syndrome in a patient with reticular dysgenesis. *J. Allergy Clin. Immunol.* **131**, 1227–1230 (2013).

12. Rissone, A. *et al.* Reticular dysgenesis–associated AK2 protects hematopoietic stem and progenitor cell development from oxidative stress. *J. Exp. Med.* **212**, 1185–1202 (2015).

13. Geltink, R. I. K., Kyle, R. L. & Pearce, E. L. Unraveling the Complex Interplay between T Cell Metabolism and Function. *Annual Review of Immunology* **36**, 461–488 (2018).

14. Skokowa, J., Dale, D. C., Touw, I. P., Zeidler, C. & Welte, K. Severe congenital neutropenias. *Nat. Rev. Dis. Prim.* **3**, (2017).

15. Hoogendijk, A. J. *et al.* Dynamic Transcriptome-Proteome Correlation Networks Reveal Human Myeloid Differentiation and Neutrophil-Specific Programming. *Cell Rep.* **29**, 2505-2519.e4 (2019).

16. Riffelmacher, T. *et al.* Autophagy-Dependent Generation of Free Fatty Acids Is Critical for Normal Neutrophil Differentiation. *Immunity* **47**, 466-480.e5 (2017).

17. Cowland, J. B. & Borregaard, N. Granulopoiesis and granules of human neutrophils. *Immunol. Rev.* **273**, 11–28 (2016).

18. Broxmeyer, H. E., O'Leary, H. A., Huang, X. & Mantel, C. The importance of hypoxia and extra physiologic oxygen shock/stress for collection and processing of stem and progenitor cells to understand true physiology/pathology of these cells ex vivo. *Current Opinion in Hematology* **22**, 273–278 (2015).

19. Hay, S. B., Ferchen, K., Chetal, K., Grimes, H. L. & Salomonis, N. The Human Cell Atlas bone marrow single-cell interactive web portal. *Exp. Hematol.* **68**, 51–61 (2018).

20. Stuart, T. *et al.* Comprehensive Integration of Single-Cell Data. *Cell* **177**, 1888-1902.e21 (2019).

21. Bak, R. O., Dever, D. P. & Porteus, M. H. CRISPR/Cas9 genome editing in human hematopoietic stem cells. *Nat. Protoc.* **13**, 358–376 (2018).

22. Aurnhammer, C. *et al.* Universal real-time PCR for the detection and quantification of adeno-associated virus serotype 2-derived inverted terminal repeat sequences. *Hum. Gene Ther. Methods* **23**, 18–28 (2012).

23. Agathocleous, M. *et al.* Ascorbate regulates haematopoietic stem cell function and leukaemogenesis. *Nature* **549**, 476–481 (2017).

24. Bray, N. L., Pimentel, H., Melsted, P. & Pachter, L. Near-optimal probabilistic RNA-seq quantification. *Nat. Biotechnol.* **34**, 525–527 (2016).

25. Love, M. I., Huber, W. & Anders, S. Moderated estimation of fold change and dispersion for RNA-seq data with DESeq2. *Genome Biol.* **15**, (2014).

26. He, L. *et al.* Detection and quantification of mitochondrial DNA deletions in individual cells by real-time PCR. *Nucleic Acids Res.* **30**, (2002).

27. Zhang, S. *et al.* Adenylate kinase AK2 isoform integral in embryo and adult heart homeostasis. *Biochem. Biophys. Res. Commun.* **546**, 59–64 (2021).

28. Bak, R. O. *et al.* Multiplexed genetic engineering of human hematopoietic stem and progenitor cells using CRISPR/Cas9 and AAV6. *Elife* **6**, 1–19 (2017).

29. Tiyaboonchai, A. *et al.* Utilization of the AAVS1 safe harbor locus for hematopoietic specific transgene expression and gene knockdown in human ES cells. *Stem Cell Res.* **12**, 630–637 (2014).

30. Baßler, J. & Hurt, E. Eukaryotic Ribosome Assembly. *Annu. Rev. Biochem.* **88**, 281–306 (2019).

31. Da Costa, L., Leblanc, T. & Mohandas, N. Diamond-Blackfan anemia. *Blood* **136**, 1262–1273 (2020).

32. Bezzerri, V. & Cipolli, M. Shwachman-Diamond Syndrome: Molecular Mechanisms and Current Perspectives. *Mol. Diagn. Ther.* **23**, 281–290 (2019).

33. Sullivan, L. B. *et al.* Supporting Aspartate Biosynthesis Is an Essential Function of Respiration in Proliferating Cells. *Cell* **162**, 552–563 (2015).

34. Birsoy, K. *et al.* An Essential Role of the Mitochondrial Electron Transport Chain in Cell Proliferation Is to Enable Aspartate Synthesis. *Cell* **162**, 540–551 (2015).

35. Whitmore, K. V. & Gaspar, H. B. Adenosine deaminase deficiency - more than just an immunodeficiency. *Front. Immunol.* **7**, (2016).

36. Grunebaum, E., Cohen, A. & Roifman, C. M. Recent advances in understanding and managing adenosine deaminase and purine nucleoside phosphorylase deficiencies. *Curr. Opin. Allergy Clin. Immunol.* **13**, 630–638 (2013).

37. Eddaoudi, A., Canning, S. L. & Kato, I. *Cellular Quiescence*. **1686**, (Springer New York, 2018).

38. Pedley, A. M. & Benkovic, S. J. A New View into the Regulation of Purine Metabolism: The Purinosome. *Trends Biochem. Sci.* **42**, 141–154 (2017).

39. Henderson, J. F. & Khoo, M. K. Y. On the Mechanism of Feedback Inhibition of Purine Biosynthesis de Novo in Ehrlich Ascites Tumor Cells in Vitro. *J. Biol. Chem.* **240**, 3104–3109 (1965).

40. Yamaoka, T. *et al.* Amidophosphoribosyltransferase limits the rate of cell growth-linked de novo purine biosynthesis in the presence of constant capacity of salvage purine biosynthesis. *J. Biol. Chem.* **272**, 17719–17725 (1997).

41. Weber, G., Donohue, J. P., Glover, J. L., Natsumeda, Y. & Prajda, N. Enzymic Capacities of Purine de Novo and Salvage Pathways for Nucleotide Synthesis in Normal and Neoplastic Tissues. *Cancer Res.* **44**, 2475–2479 (1984).

42. Mayer, D. *et al.* Expression of key enzymes of purine and pyrimidine metabolism in a hepatocyte-derived cell line at different phases of the growth cycle. *J. Cancer Res. Clin. Oncol.* **116**, 251–258 (1990).

43. Admyre, T. *et al.* Inhibition of AMP deaminase activity does not improve glucose control in rodent models of insulin resistance or diabetes. *Chem. Biol.* **21**, 1486–1496 (2014).

44. Plaideau, C. *et al.* Effects of pharmacological AMP deaminase inhibition and ampd1 deletion on nucleotide levels and AMPK activation in contracting skeletal muscle. *Chem. Biol.* **21**, 1497–1510 (2014).

45. Carson, D. A., Lakow, E., Wasson, D. B. & Kamatani, N. Lymphocyte dysfunction caused by deficiencies in purine metabolism. *Immunol. Today* **2**, 234–238 (1981).

46. Cohen, A., Gudas, L. J., Ammann, A. J., Staal, G. E. & Martin, D. W. Deoxyguanosine triphosphate as a possible toxic metabolite in the immunodeficiency associated with purine nucleoside phosphorylase deficiency. *J. Clin. Invest.* **61**, 1405–1409 (1978).

47. Howell, N. & Sager, R. Cytoplasmic genetics of mammalian cells: Conditional sensitivity to mitochondrial inhibitors and isolation of new mutant phenotypes. *Somatic Cell Genet.* **5**, 833–845 (1979).

48. Hershfield, M. *Adenosine Deaminase Deficiency*. *GeneReviews®* (1993).

49. Nicholls, D. G. & Ferguson, S. J. *Bioenergetics (4th Edition)*. *Academic Press* (2013).

50. Nobuaki Ogasawara, Haruko Goto, Yasukazu Yamada, Tomomasa Watanabe & Tomiko Asano. AMP deaminase isozymes in human tissues. *Biochim. Biophys. Acta - Gen. Subj.* **714**, 298–306 (1982).

51. Smolenski, R. T. *et al.* AMP deaminase 1 gene polymorphism and heart disease - A genetic association that highlights new treatment. *Cardiovascular Drugs and Therapy* **28**, 183–189 (2014).

52. Rybakowska, I. M., Bakuła, S. & Kaletha, K. Isozymes of AMP-Deaminase in Muscles Myasthenia Gravis Patients. *Int. J. Pept. Res. Ther.* **22**, 511–515 (2016).

53. Zhan, X. *et al.* Adenosine monophosphate deaminase 3 null mutation causes reduction of naive T cells in mouse peripheral blood. *Blood Adv.* **4**, 3594–3605 (2020).

54. Dieck, C. L. & Ferrando, A. Genetics and mechanisms of NT5C2-driven chemotherapy resistance in relapsed ALL. *Blood* **133**, 2263–2268 (2019).

55. Moriyama, T. *et al.* Mechanisms of NT5C2-mediated thiopurine resistance in acute lymphoblastic leukemia. *Mol. Cancer Ther.* **18**, 1887–1895 (2019).

56. Maslah, N. *et al.* Adenylate kinase 2 expression and addiction in T-ALL. *Blood Adv.* **5**, 700–710 (2021).

57. Six, E. *et al.* AK2 deficiency compromises the mitochondrial energy metabolism required for differentiation of human neutrophil and lymphoid lineages. *Cell Death Dis.* **6**, e1856 (2015).

58. An, S., Kumar, R., Sheets, E. D. & Benkovic, S. J. Reversible compartmentalization of de novo purine biosynthetic complexes in living cells. *Chemtracts* **20**, 501–502 (2008).

59. French, J. B. *et al.* Spatial colocalization and functional link of purinosomes with mitochondria. *Science (80-.).* **351**, 733–737 (2016).

60. McKean, W. B., Toshniwal, A. G. & Rutter, J. A time to build and a time to burn: glucose metabolism for every season. *Mol. Cell* **81**, 642–644 (2021).

61. Luengo, A. *et al.* Increased demand for NAD+ relative to ATP drives aerobic glycolysis. *Mol. Cell* **81**, 691-707.e6 (2021).

62. Guo, Z., Kozlov, S., Lavin, M. F., Person, M. D. & Paull, T. T. ATM activation by oxidative stress. *Science (80-.).* **330**, 517–521 (2010).

63. Finkel, T. & Holbrook, N. J. Oxidants, oxidative stress and the biology of ageing. *Nature* **408**, 239–247

(2000).

64. Rajasekaran, N.-S. Reductive Stress: Neglected Science. *Antioxid. Redox Signal.* ars.2020.8114 (2020). doi:10.1089/ars.2020.8114

65. Xiao, W. & Loscalzo, J. Metabolic Responses to Reductive Stress. *Antioxidants Redox Signal.* **32**, 1330–1347 (2020).

66. Veliova, M., Petcherski, A., Liesa, M. & Shirihai, O. S. The biology of lipid droplet-bound mitochondria. *Seminars in Cell and Developmental Biology* **108**, 55–64 (2020).

Figure Legend

Figure 1. Single cell RNA-seq analysis of Reticular Dysgenesis patient bone marrow.

(A) UMAP of bone marrow cells from 8 healthy donors (HD) and 2 Reticular Dysgenesis patients (RD) identified 22 clusters. Cluster of apoptotic cells (frequency <3% in all samples) was removed from downstream analysis. HSC, hematopoietic stem cells; CMP, common myeloid progenitor cells; CLP, common lymphoid progenitor cells; MEP, Megakaryocyte–erythroid progenitor cells; PM/MC, promyelocytes/myelocytes; NKT, NK T cell; ERP, erythroid progenitor cells. (B, C) Distribution of HD and RD bone marrow cells across all clusters. RD samples showed a higher frequency in HSPC clusters (HSC, CMP, CLP, EarlyProB, ProB and MEP), and lower frequency in mature myeloid and lymphoid clusters, including monocytes, T cells and NK cells. (D) AK1 and AK2 mRNA levels in RD and HD bone marrow cells. AK1 expression is largely restricted to the erythrocyte lineage past MEP stage, whereas AK2 is broadly expressed in all lineages. The RD patients in this study suffer from a point mutation in AK2 in a late exon (exon 6), therefore AK2 transcripts could still be detected in RD samples. (E) GO enrichment analysis of down regulated DEGs in RD vs HD cells. Node size is proportional to number of DEGs. Edge width is proportional to number of overlapping genes between gene sets. Multiple pathways related to RNA metabolism, ribosomal biogenesis and cell cycle progression are enriched in HSPC clusters (HSC, CMP, CLP and ProB).

Figure 2. Flow cytometry analysis of RD patient bone marrow.

(A) Flow cytometry analysis of the myeloid lineage of healthy donor and RD patient bone marrow. (B) Bar graphs showing percentages of granulocytic committed cells within the myeloid lineage, and percentages of promyelocytes and neutrophils within the granulocytic committed cells, in healthy donor and RD patients.

Figure 3. Biallelic AK2 knock out HSPCs recapitulate RD myelopoiesis defects.

(A) Design of AK2 guide RNA targeting the LID domain and homologous DNA donors with GFP and BFP reporters. (B) GFP+BFP+ fraction maintains donor integration. (C) AK2 protein expression is absent in the GFP+BFP+ fraction of AK2 CRISPR edited HSPCs. (D) Representative flow cytometry plot of AK2-/- and AAVS1-/- HSPC differentiation along the granulocytic lineage. (E) Box plot of percentage of HLA-DR- HSPCs differentiated along the granulocytic lineage. (F) Box plots of percentages of PMs, MCs and NPs within the HLA-DR- granulocytic committed cells. (G) Box plot of cell proliferation of AK2-/- vs AAVS1-/- HSPCs after 7 day culture in the neutrophil differentiation media. (H) Box plots of the number of PMs, MCs and NPs yielded from 1 HSPC after 7 day culture in the neutrophil differentiation media.

Figure 4. Energy metabolism and protein synthesis during normal myelopoiesis.

(A, B) Measurement of oxygen consumption rate (OCR) and extracellular acidification rate (ECAR) in a Seahorse mito stress test assay. Oligomycin, FCCP and rotenone/antimycin A were sequentially injected into cell wells, and OCR and ECAR were measured before and after each drug injection. (C-F) Bar graphs showing baseline OCR (C), maximal OCR (D), spare respiratory capacity, as calculated by maximal OCR - baseline OCR (E), and baseline ECAR (F) for each cell type. (G) Bar graph of mitochondrial copy numbers as quantified by the fraction of mt-ND1 copy number and nuclear B2M copy number in each cell type. (H) Heatmap of the expression of ribosomal subunit genes in each cell type. (G) Ribosomal RNA content in each cell type, quantified by Pyronin Y staining. (H) Nascent peptide synthesis rate in each cell type, quantified by OP-puromycin incorporation.

Figure 5. Metabolomics profiling.

Box plots showing relative abundance of AMP, NAD+ glucose 6-phosphate, phosphoenolpyruvate (PEP) and malate; and relative ratios of AMP/ADP, AMP/ATP, NADH/NAD+ and GSH/GSSG, in AK2-/- vs AAVS1-/- PMs, MCs, and NPs.

Figure 6. Mitochondrial metabolism of AK2 depleted PMs.

(A-B) Seahorse mito stress test assay of AAVS1-/- and AK2-/- PMs. Oligomycin, FCCP and rotenone/antimycin A were sequentially injected into cell wells, and OCR and ECAR were measured before and after each drug injection. (C-F) Bar graphs showing baseline OCR (C), maximal OCR (D), spare respiratory capacity, as calculated by maximal OCR - baseline OCR (E), and baseline ECAR (F) for AK2-/- vs AAVS1-/- PMs. (G) Bar graph of mitochondrial copy number of AK2-/- vs AAVS1-/- PMs and MCs. (H) Mitochondrial membrane potential of AK2-/- vs AAVS1-/- PMs, as measured by TMRM staining.

Figure 7. AK2 depletion disrupts purine metabolism and protein synthesis.

(A-B) Box plots showing relative abundance of aspartate and IMP in in AAVS1-/- and AK2-/- cells. (D) Volcano plots showing down-regulation of ribosomal subunit genes in AK2-/- PMs and MCs. (E) Ribosomal RNA contents of AK2-/- vs AAVS1-/- MCs and NPs, quantified by Pyronin Y staining. (F) Nascent peptide synthesis rate of AK2-/- vs AAVS1-/- PMs, quantified by OP-puromycin incorporation.

Figure 8. AMP deamination causes IMP accumulation in AK2 depleted cells.

(A-B) Bar graphs showing proliferation and granulocyte yield of AAVS1-/- and AK2-/- HSPCs differentiated in MEM alpha media containing no nucleosides (none) and with mixed nucleosides and deoxynucleosides (all). (C-D) Bar graphs showing proliferation and granulocyte yield of AAVS1-/- and AK2-/- HSPCs differentiated in MEM alpha media containing no nucleosides (none), with 40mg/L adenosine supplementation (aden), and with 40mg/L guanosine supplementation (guan). (E-F) Bar graphs showing proliferation and granulocyte yield of AAVS1-/- and AK2-/- HSPCs treated with DMSO control or 20μM AMPD inhibitor (AMPDi). (G-H) Box plots showing relative abundance of IMP and AMP in AAVS1-/- and AK2-/- cells treated with DMSO control or 20μM AMPD inhibitor (AMPDi).

Figure S1. Lineage specific marker gene expression in cell populations.

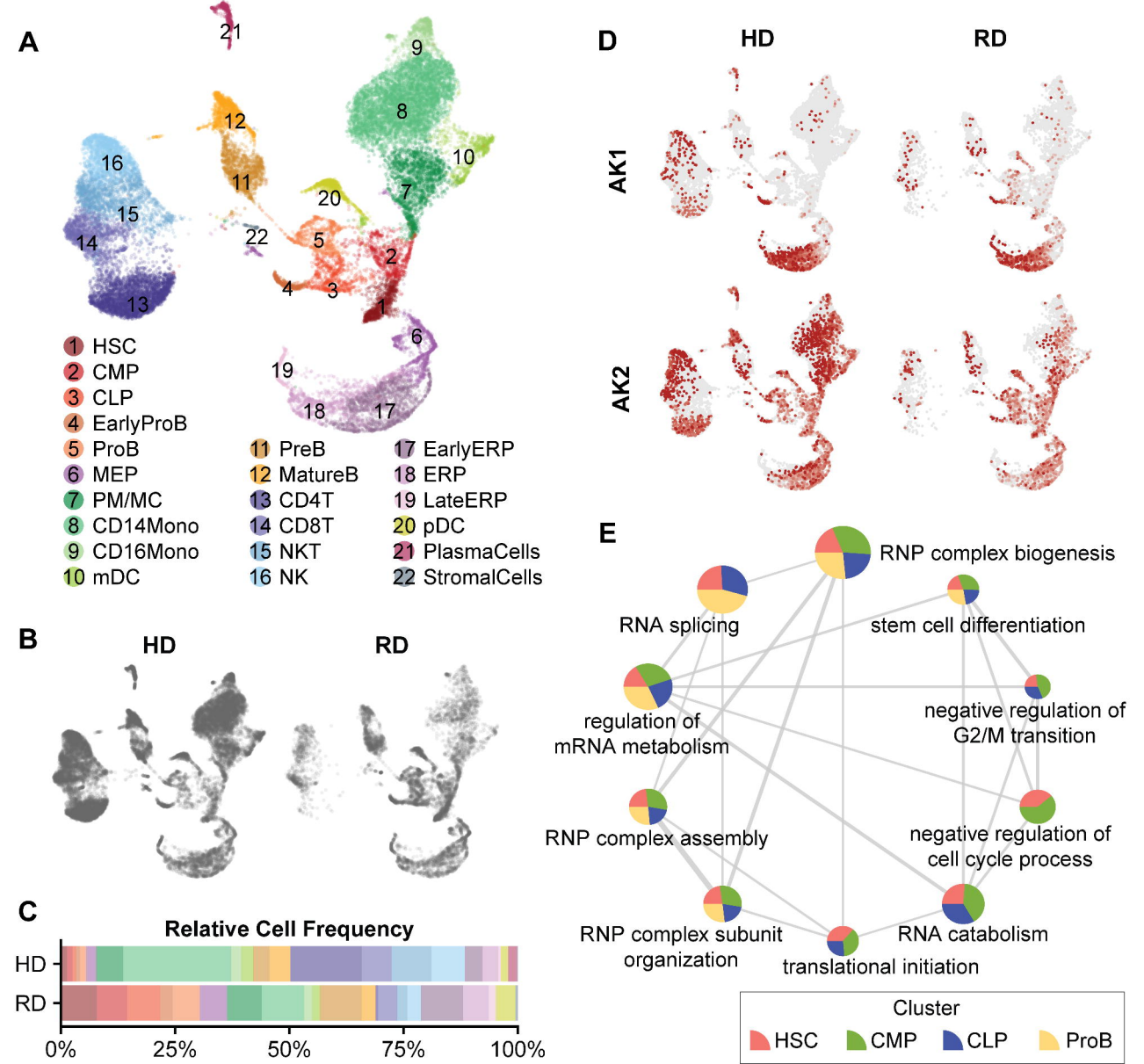
A
1 HSC
2 CMP
3 CLP
4 EarlyProB
5 ProB
6 MEP
7 PM/MC
8 CD14Mono
9 CD16Mono
10 mDC
11 PreB
12 MatureB
13 CD4T
14 CD8T
15 NKT
16 NK
17 EarlyERP
18 ERP
19 LateERP
20 pDC
21 PlasmaCells
22 StromalCells
B
HD
RD
C
Relative Cell Frequency
HD
RD
0%
25%
50%
75%
100%
D
HD
RD
AK1
AK2
E
RNP complex biogenesis
RNA splicing
stem cell differentiation
regulation of mRNA metabolism
negative regulation of G2/M transition
RNP complex assembly
negative regulation of cell cycle process
RNP complex subunit organization
RNA catabolism
translational initiation
Cluster
HSC
CMP
CLP
ProB

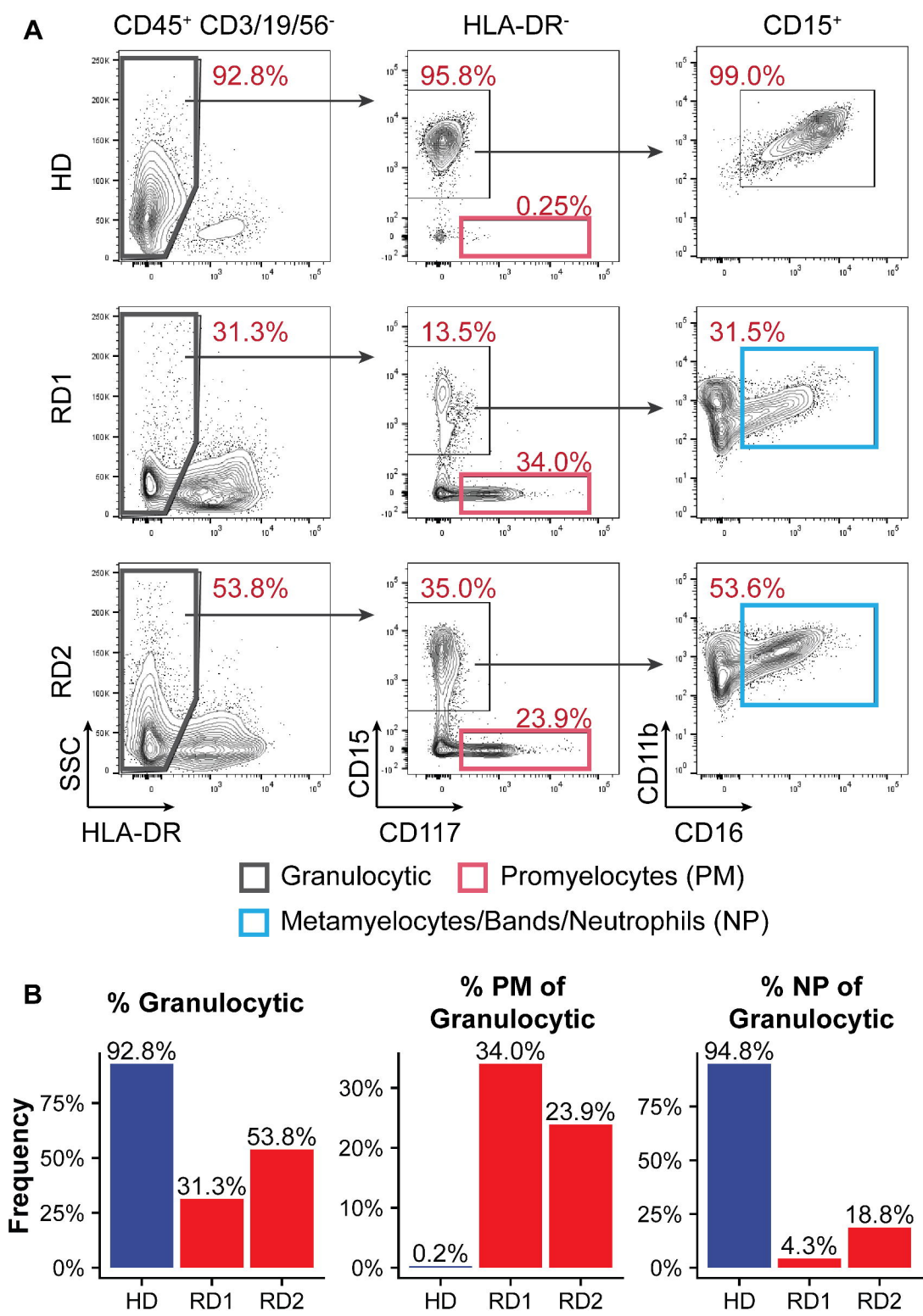
A
CD45+ CD3/19/56-
HLA-DR-
CD15+
HD
RD1
RD2
92.8%
95.8%
99.0%
0.25%
31.3%
13.5%
31.5%
34.0%
53.8%
35.0%
53.6%
23.9%
SSC
HLA-DR
CD15
CD117
CD11b
CD16
Granulocytic
Promyelocytes (PM)
Metamyelocytes/Bands/Neutrophils (NP)
B
% Granulocytic
% PM of Granulocytic
% NP of Granulocytic
Frequency
92.8%
31.3%
53.8%
0.2%
34.0%
23.9%
94.8%
4.3%
18.8%
HD
RD1
RD2

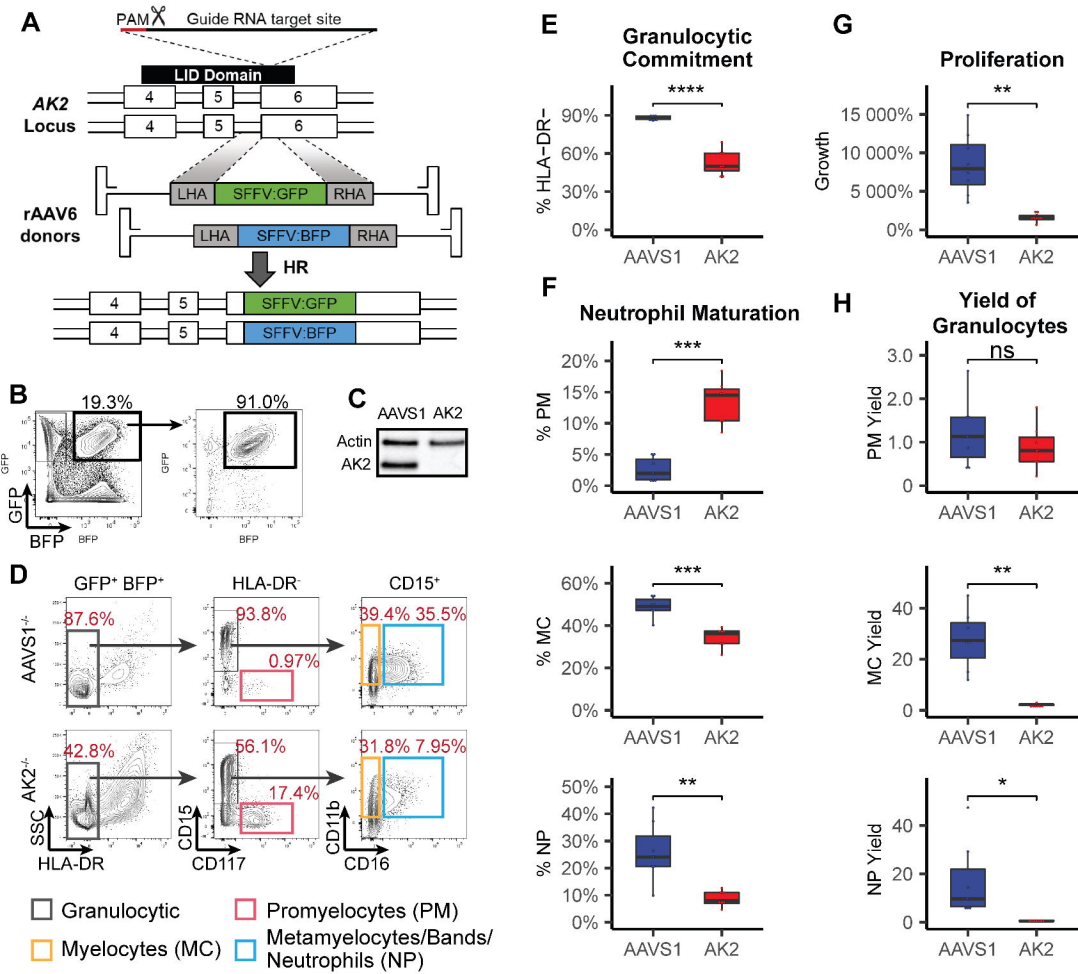
A
PAM
Guide RNA target site
LID Domain
AK2 Locus
4
5
6
rAAV6 donors
LHA
SFFV:GFP
RHA
SFFV:BFP
HR
B
19.3%
91.0%
GFP
BFP
C
AAVS1 AK2
Actin
AK2
D
GFP+ BFP+
HLA-DR-
CD15+
AAVS1-/-
AK2-/-
87.6%
93.8%
0.97%
39.4% 35.5%
42.8%
56.1%
17.4%
31.8% 7.95%
SSC
HLA-DR
CD15
CD117
CD11b
CD16
Granulocytic
Promyelocytes (PM)
Myelocytes (MC)
Metamyelocytes/Bands/ Neutrophils (NP)
E
Granulocytic Commitment
% HLA-DR-
****
AAVS1
AK2
F
Neutrophil Maturation
% PM
***
% MC
***
% NP
**
G
Proliferation
Growth
**
H
Yield of Granulocytes
PM Yield
ns
MC Yield
**
NP Yield
*

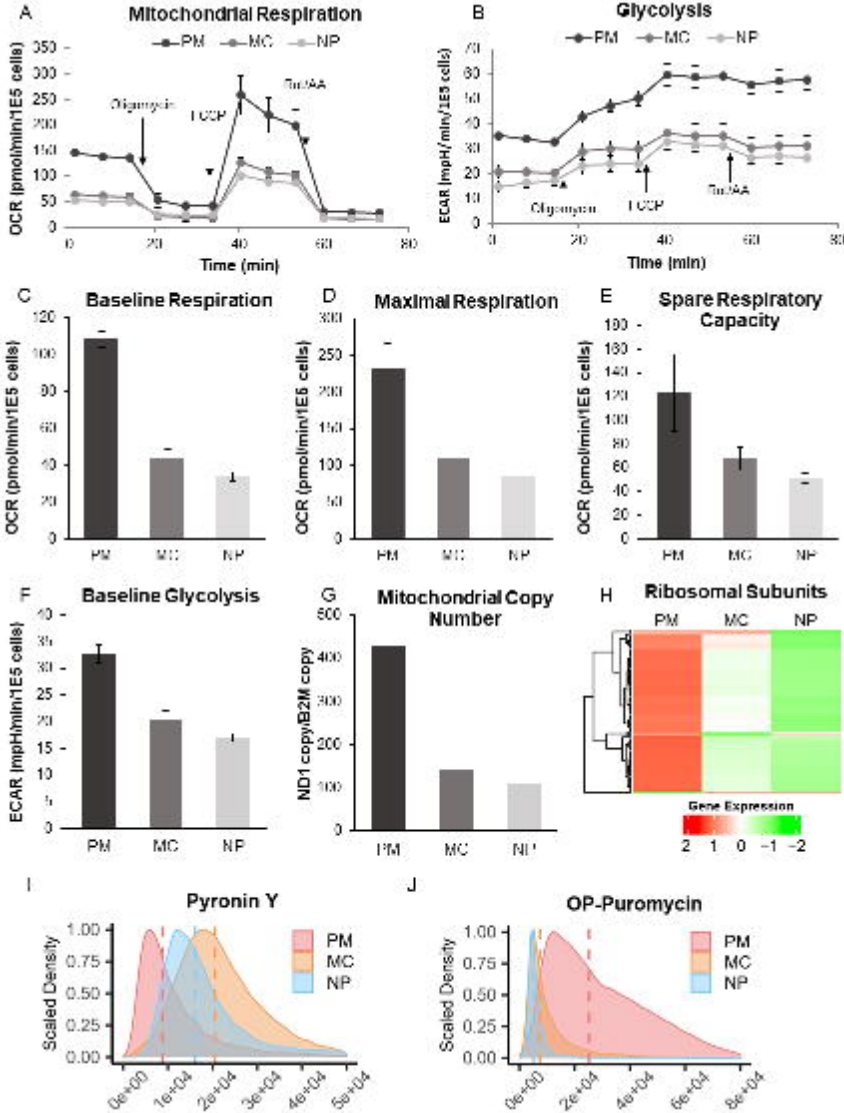
A
Mitochondrial Respiration
PM
MC
NP
OCR (pmol/min/1E5 cells)
Oligomycin
FCCP
Rot/AA
Time (min)
B
Glycolysis
ECAR (mpH/min/1E5 cells)
Oligomycin
FCCP
Rot/AA
Time (min)
C
Baseline Respiration
OCR (pmol/min/1E5 cells)
D
Maximal Respiration
OCR (pmol/min/1E5 cells)
E
Spare Respiratory Capacity
OCR (pmol/min/1E5 cells)
F
Baseline Glycolysis
ECAR (mpH/min/1E5 cells)
G
Mitochondrial Copy Number
ND1 copy/B2M copy
H
Ribosomal Subunits
Gene Expression
I
Pyronin Y
Scaled Density
J
OP-Puromycin
Scaled Density

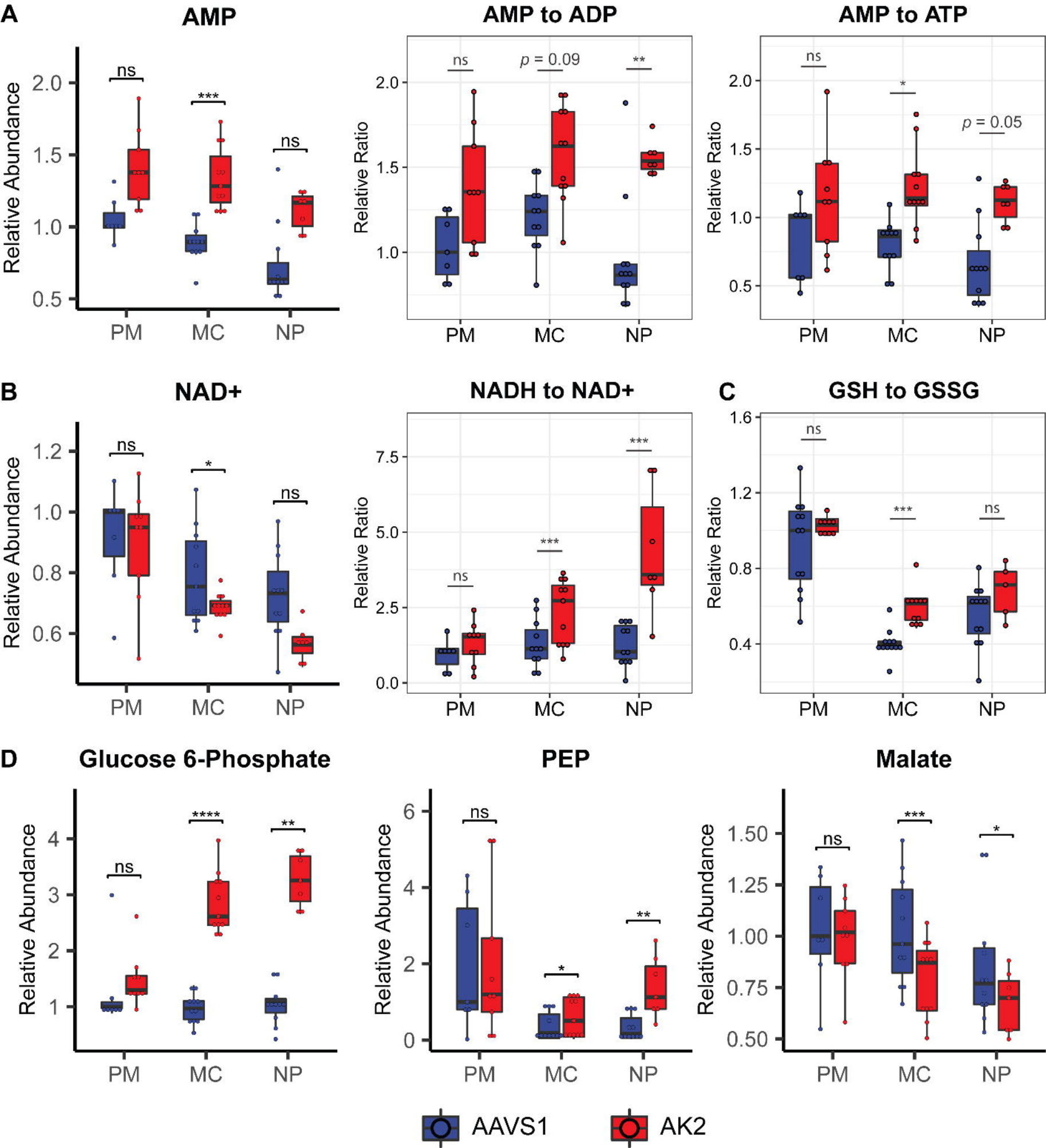
A
AMP
Relative Abundance
ns
***
ns
PM
MC
NP
AMP to ADP
Relative Ratio
ns
p = 0.09
**
AMP to ATP
Relative Ratio
ns
*
p = 0.05
B
NAD+
Relative Abundance
ns
*
ns
NADH to NAD+
Relative Ratio
ns
***
***
C
GSH to GSSG
Relative Ratio
ns
***
ns
D
Glucose 6-Phosphate
Relative Abundance
ns
****
**
PEP
Relative Abundance
ns
*
**
Malate
Relative Abundance
ns
***
*
AAVS1
AK2

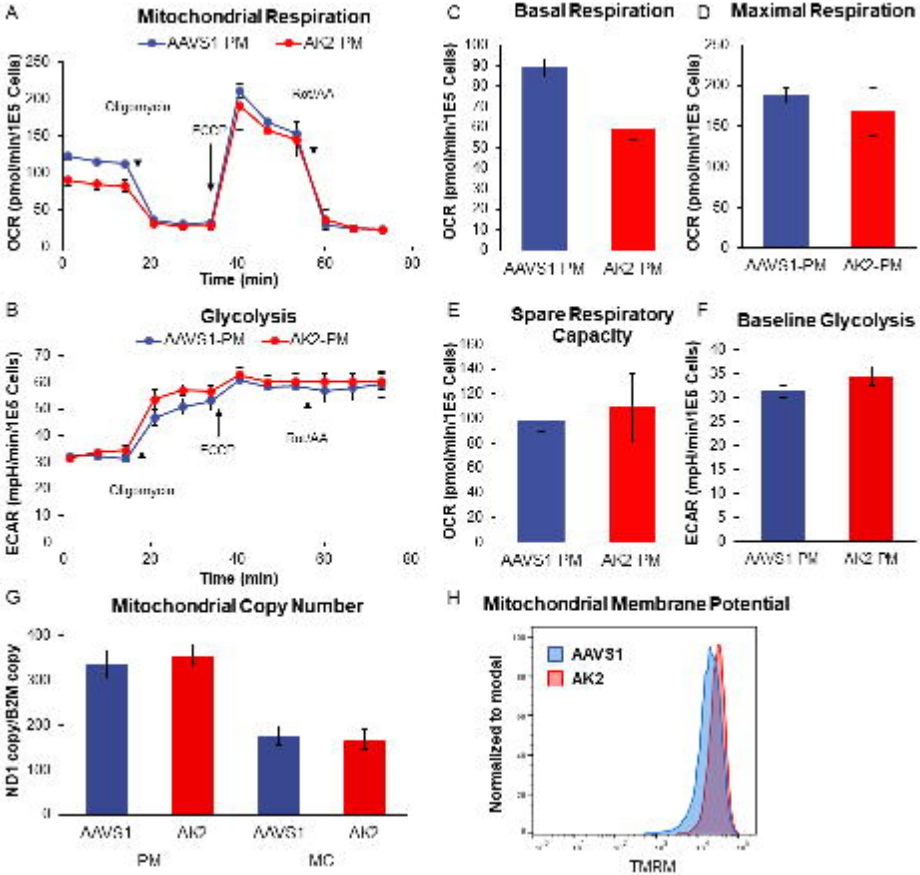
A
Mitochondrial Respiration
AAVS1 PM
AK2 PM
OCR (pmol/min/1E5 Cells)
Oligomycin
FCCP
Rot/AA
Time (min)
B
Glycolysis
AAVS1-PM
AK2-PM
ECAR (mpH/min/1E5 Cells)
Oligomycin
FCCP
Rot/AA
Time (min)
C
Basal Respiration
OCR (pmol/min/1E5 Cells)
AAVS1 PM
AK2 PM
D
Maximal Respiration
OCR (pmol/min/1E5 Cells)
AAVS1-PM
AK2-PM
E
Spare Respiratory Capacity
OCR (pmol/min/1E5 Cells)
AAVS1 PM
AK2 PM
F
Baseline Glycolysis
ECAR (mpH/min/1E6 Cells)
AAVS1 PM
AK2 PM
G
Mitochondrial Copy Number
ND1 copy/B2M copy
AAVS1
AK2
AAVS1
AK2
PM
MC
H
Mitochondrial Membrane Potential
AAVS1
AK2
Normalized to model
TMRM

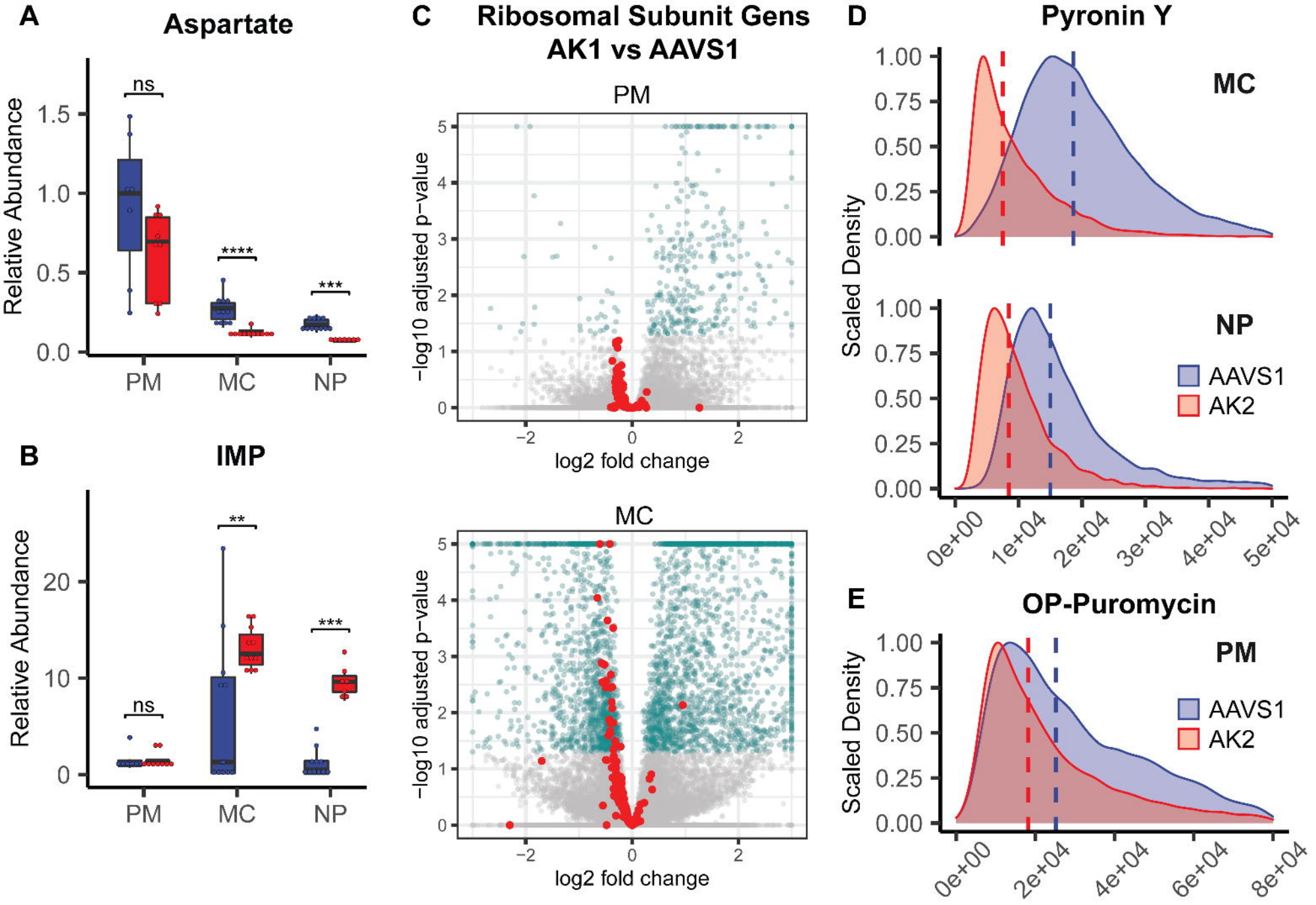
A
Aspartate
Relative Abundance
ns
****
***
PM
MC
NP
B
IMP
Relative Abundance
ns
**
***
PM
MC
NP
C
Ribosomal Subunit Gens
AK1 vs AAVS1
PM
−log10 adjusted p−value
log2 fold change
MC
−log10 adjusted p−value
log2 fold change
D
Pyronin Y
MC
NP
Scaled Density
AAVS1
AK2
E
OP-Puromycin
PM
Scaled Density
AAVS1
AK2

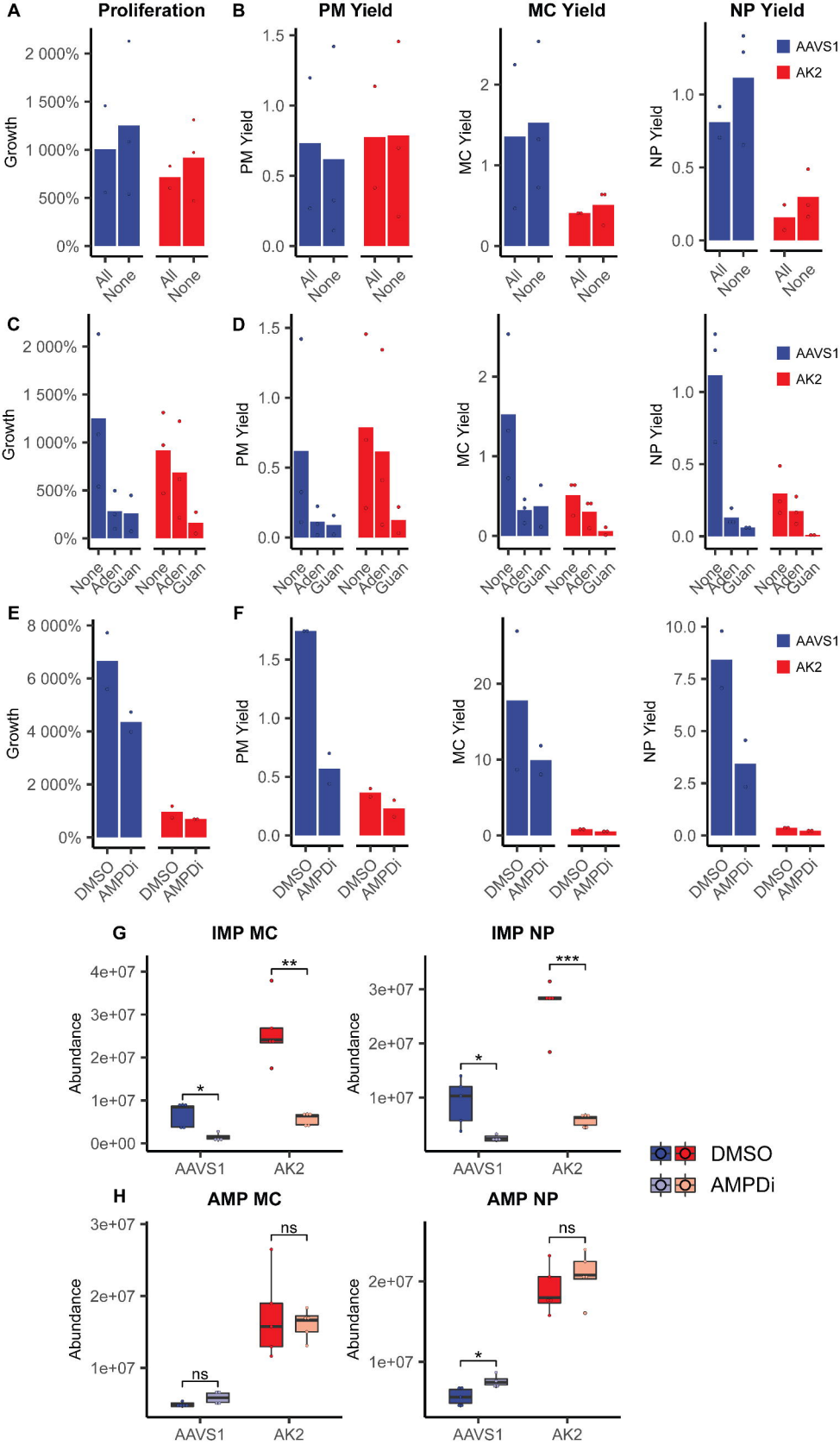
A
Proliferation
Growth
2 000%
1 500%
1 000%
500%
0%
All
None
B
PM Yield
1.5
1.0
0.5
0.0
MC Yield
2
1
0
NP Yield
AAVS1
AK2
C
None
Aden
Guan
D
E
8 000%
6 000%
4 000%
2 000%
0%
DMSO
AMPDi
F
20
10
10.0
7.5
5.0
2.5
G
IMP MC
IMP NP
Abundance
4e+07
3e+07
2e+07
1e+07
0e+00
*
**
***
AAVS1
AK2
DMSO
AMPDi
H
AMP MC
AMP NP
ns

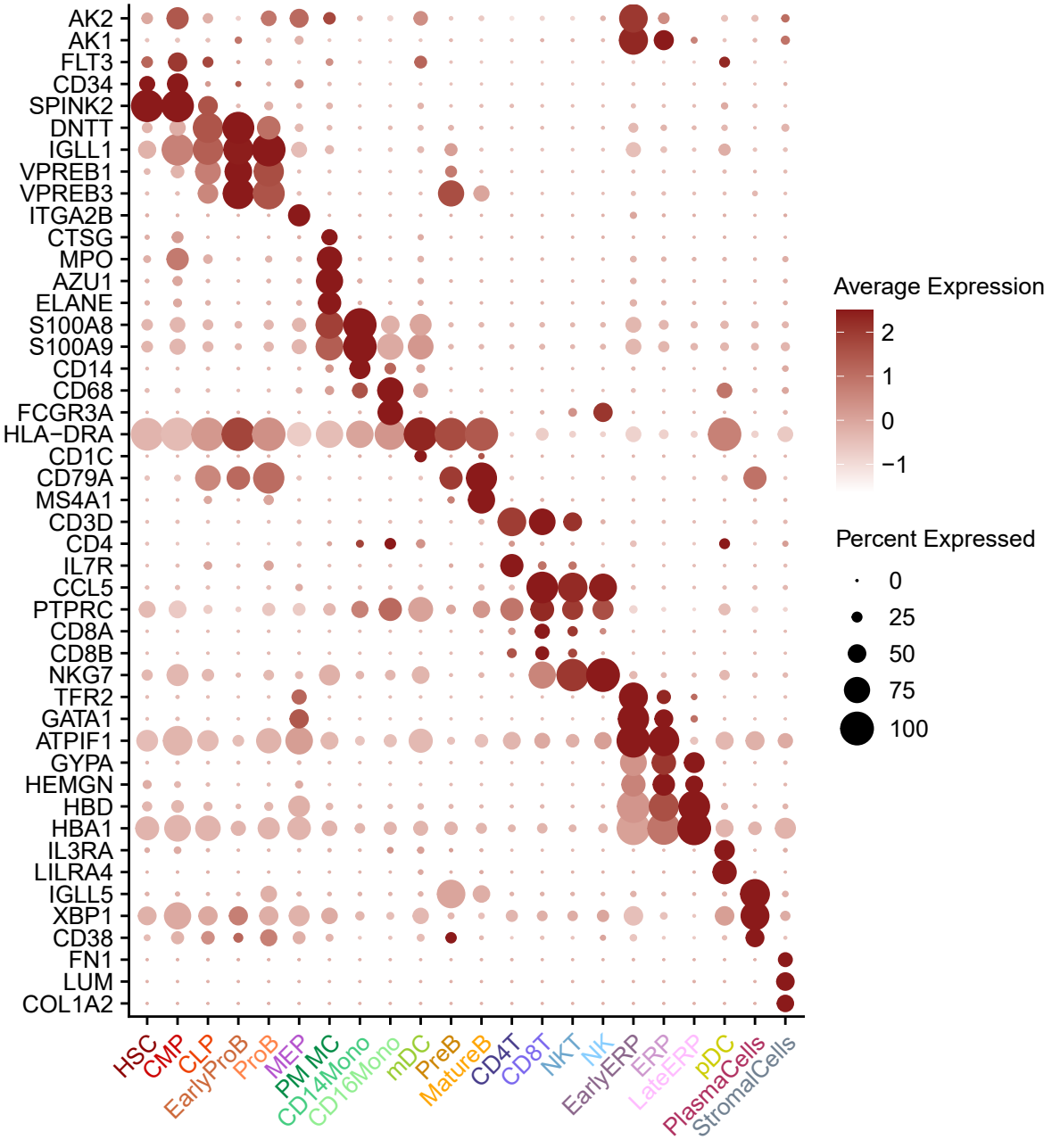
AK2
AK1
FLT3
CD34
SPINK2
DNTT
IGLL1
VPREB1
VPREB3
ITGA2B
CTSG
MPO
AZU1
ELANE
S100A8
S100A9
CD14
CD68
FCGR3A
HLA−DRA
CD1C
CD79A
MS4A1
CD3D
CD4
IL7R
CCL5
PTPRC
CD8A
CD8B
NKG7
TFR2
GATA1
ATPIF1
GYPA
HEMGN
HBD
HBA1
IL3RA
LILRA4
IGLL5
XBP1
CD38
FN1
LUM
COL1A2
HSC
CMP
CLP
EarlyProB
ProB
MEP
PM MC
CD14Mono
CD16Mono
mDC
PreB
MatureB
CD4T
CD8T
NKT
NK
EarlyERP
ERP
LateERP
pDC
PlasmaCells
StromalCells
Average Expression
2
1
0
−1
Percent Expressed
0
25
50
75
100